

Rotatable Array-Aided Hybrid Beamforming for Integrated Sensing and Communication

Zequan Wang, Liang Yin, Yitong Liu, Yunan Sun, and Hongwen Yang

Abstract—Integrated Sensing and Communication (ISAC) is one of the pivotal supporting technologies for next-generation wireless communication networks. As an emerging technical means, the new six-dimensional movable antenna (6DMA) system can effectively improve the communication and sensing performance of ISAC systems. However, related research on the architecture based on three-dimensional rotatable antennas (RA) remains relatively limited. Especially under the influence of non-ideal channel characteristics, how to balance system performance and hardware cost control through beamforming technology in non-ideal channels has become a crucial issue to be solved urgently. Given the significant advantages of hybrid beamforming technology in balancing system performance and hardware complexity, this paper focuses on the channel model considering effective aperture loss under the RA architecture and studies the sub-connected hybrid beamforming design for multi-user ISAC systems. Aiming at the non-convex nature with coupled variables in this problem, this paper first transforms the complex fractional objective function using the Fractional Programming (FP) framework, and then proposes an algorithm based on the Alternating Optimization (AO) architecture, which achieves optimization by alternately solving five subproblems. Among them, the closed-form update expression of the array rotation angle is derived through the Karush-Kuhn-Tucker (KKT) conditions, and a two-stage Gradient Ascent (GA) based method is proposed to optimize the antenna rotation angle. Simulation results show that compared with the traditional fixed-position antenna (FPA), the proposed method can significantly improve the overall performance of the system.

Index Terms—Integrated sensing and communication (ISAC), 6D movable antenna, antenna rotation optimization, alternating optimization, hybrid analog-digital beamforming.

I. INTRODUCTION

Integrated sensing and communication (ISAC) has become a highly promising technology in the sixth-generation (6G) wireless network [1] [2]. Its core advantage is the ability to share hardware platforms and signal bandwidths. This helps achieve efficient resource use for communication and radar sensing. This feature not only greatly improves spectrum efficiency, but also cuts hardware costs a lot [3]. Because of these advantages, ISAC has shown great potential in many applications. These include vehicle-to-everything (V2X), industrial internet of things (IIoT), and environmental monitoring [2]. In addition, ISAC has attracted wide attention from both academia and industry. It integrates a series of emerging wireless technologies, such as reconfigurable intelligent surface (RIS) [4]

Z. Wang, L. Yin, Y. Liu, Y. Sun, and H. Yang are with the School of Information and Communication Engineering, Beijing University of Posts and Telecommunications, Beijing, 100876, China (e-mail: {zequanwang, YinL, liuyitong, sunyunan, yanghong}@bupt.edu.cn).

(Corresponding author: Liang Yin)

[5], unmanned aerial vehicle (UAV) [6], and non-orthogonal multiple access (NOMA) [7] [8]. This further enhances its performance and application potential.

With the continuous evolution of 6G communication systems, the large-scale application of high-frequency millimeter wave and large antenna array has become an irreversible technological trend. By increased antenna numbers, large antenna array can significantly improve beamforming gain and enhance spatial resolution, thereby effectively improving the communication and sensing performance. However, the fully-digital beamforming scheme requires each antenna unit to be equipped with an independent radio frequency chain, which makes the deployment of large antenna array face the challenge of a sharp rise in hardware costs and power consumption, seriously restricting its popularization and application in practical scenarios. In contrast, the hybrid beamforming [9] [10], relying on a small number of RF chains and an analog front end consisting of phase shifters (PSs), has been considered as a promising technique to achieve a good trade-off between cost and communication performance.

Based on the front end design of PS circuits, the hybrid beamformer can be categorized into fully-connected structures and sub-connected structures [11]. In the fully-connected structure, all RF chains are connected to all antenna elements through PSs, which endows a higher system degree of design freedom (DoFs). However, it also results in high hardware costs and energy consumption overheads, which are particularly prominent in the scenario of large-scale antenna array in millimeter wave systems. In contrast, the sub-connected structure, by connecting each RF chain only to a part of the antenna elements, has higher energy efficiency and is easier for engineering implementation. To improve system performance under the constraint of a limited number of RF chains, numerical optimization algorithms have been proposed [9] [7] [13]. [9] designs a fully-digital beamformer, then iteratively optimizes the hybrid beamformer to gradually approximate the performance of the fully-digital solution. [7] proposes a method to directly optimize the hybrid beamformer in an iterative manner. [13] introduces a continuous auxiliary variable to replace the beamforming variable with unit modulus constraint, optimizes the auxiliary variable, extracts its phase, and finally obtains the design result of the beamformer. Nevertheless, most of the existing fully-connected and sub-connected hybrid beamforming schemes rely on fixed position antennas (FPA), and the transmitter/receiver fail to fully exploit the spatial variation of wireless channels, thus ignoring the gain improvement that can be brought about by dynamic channel adjustment.

ISAC aims primarily to enhance communication capacity and sensing ability [14]. In recent years, movable antenna (MA) and six-dimensional MA (6DMA) technologies have been proposed to improve the performance of wireless communication [20]- [19]. Specifically, compared with the traditional MA which can only dynamically adjust the position of antenna elements within a specific feasible region, the 6DMA can flexibly regulate its spatial position and rotation angle, and integrate the DoFs of the antenna in three-dimensional (3D) position and rotation dimensions, thus providing customized sensing and communication services more efficiently [16]- [19]. Several studies have investigated the integration of MA to enhance communication capacity [20]- [27]. Specifically, the authors analyze the performance of the MA enabled wireless communication system in [20]. They derive closed-form expressions for channel gain under deterministic and random channel environments, verifying the effectiveness of MA in improving channel capacity. [21] investigates a MA-enabled full-duplex ISAC system, which considers the scenario of user uplink and downlink transmissions and sets the sum of user uplink/downlink communication rates and target sensing rate as the optimization objective. The authors in [22] conduct research on ISAC systems with clutter interference, deriving in detail the derivative of channel gain with respect to antenna position, and optimizing the antenna position based on the gradient ascent method. The authors in [23] [24] propose a scheme for MA aided multi-user communication scenarios under hybrid precoding design. The authors in [25] study the trade-off between communication and sensing in MA-enabled ISAC system, and adopts the Particle Swarm Optimization (PSO) algorithm to determine the optimal position of the antenna. [26] explores the application of MA in multi-target detection, and the results show that MA can significantly reduce transmission power while ensuring communication and sensing performance. [27] investigates multi-user communication systems supported by the collaboration of RIS and MA.

Although the advantages of MA in ISAC systems have been validated, effectively enhancing communication and sensing performance by optimizing antenna positions remains a challenging issue. The main difficulty arises from the complex expression of the wireless channel with respect to the positions of the antennas, causing non-convex expressions involving coupling variables. Existing studies mostly focus on MA-enabled ISAC systems with adjustable positions. In contrast, the investigation of ISAC systems considering antenna rotatability is still in its infancy. Generally, antenna rotation can optimize beam pointing more flexibly, and can provide customized sensing and communication services more efficiently, especially when considering an accurate channel model that includes effective aperture [28]. To this end, this paper studies the hybrid beamforming design for multi-user multi-input-single-output (MU-MISO) ISAC systems based on rotatable antennas, aiming to reduce hardware cost and complexity while improving the communication and sensing performance of the system. To the best of the authors' knowledge, this is among the first works to explore RA-based ISAC. The main contributions of this paper are summarized as follows.

- 1) We study a hybrid beamforming design for a RA enabled ISAC system. In this design, to balance sensing accuracy and communication efficiency, the goal is to maximize the weighted sum of each user's communications rate and the target sensing rate by jointly optimizing the transmit digital beamformer, transmit analog beamformer, receive beamformer, and antenna rotation angles.
- 2) We propose an alternating optimization (AO) based framework to solve the formulated problem, which enables the direct design of the hybrid beamformer. Specifically, the minimum mean square error (MMSE) filtering method is first adopted to optimize the receive beamformer. Then, Facilitated by fractional programming (FP), the remaining problem is decomposed into four subproblems to handle the coupled variables. Among them, an algorithm based on singular value decomposition (SVD) and Karush-Kuhn-Tucker (KKT) conditions is proposed to solve the analog beamforming problem, and the gradient ascent (GA) method is used to solve the array rotation angle optimization problem.
- 3) We perform numerical simulations to evaluate the performance of RA in ISAC system with our proposed algorithm, and demonstrate the performance trade-off between communication and sensing. Simulation results confirm that adopting RA with our proposed algorithm significantly enhances both sensing and communication performance with our proposed algorithm. Moreover, under certain practical conditions, the proposed scheme with sub-connected RA yields a higher sum rate compared to the fully-connected FPA array.

Notation: a/A , \mathbf{a} , \mathbf{A} , and \mathcal{A} denote a scalar, a vector, a matrix, and a set, respectively. $(\cdot)^T$, $(\cdot)^H$, $\|\cdot\|_2$, $|\cdot|$, $\|\cdot\|_F$, $\text{Tr}\{\cdot\}$, and $\text{Rank}\{\cdot\}$ denote the transpose, conjugate transpose, Euclidean norm, absolute value, Frobenius matrix norm, trace, and rank, respectively. $j = \sqrt{-1}$ represents the imaginary unit. $\mathbb{C}^{M \times N}$ and $\mathbb{R}^{M \times N}$ are the sets for complex and real matrices of $M \times N$ dimensions, respectively. \mathbf{I}_N is the identity matrix of order N . $\mathcal{CN}(0, \sigma^2)$ represents the circularly symmetric complex Gaussian (CSCG) distribution with mean zero and covariance σ^2 . Finally, $[\cdot]_{(m,n)}$ denotes the (m, n) -th element of a matrix.

II. SYSTEM MODEL

As illustrated in Fig. 1, we consider an RA-enabled far-field MU-MISO system. The system comprises a dual functional radar and communication (DFRC) BS serving K single-FPA users, sensing one target, and considering C clutters as interference for sensing. We consider a bistatic setup at the BS, which sparsified Tx and Rx to avoid challenging issues in full-duplex mode. Thus, self-interference (SI) can be significantly suppressed through the Tx and Rx are sufficiently separated. Therefore, in this paper, we assume that the SI is completely cancellation. To reduce power consumption and hardware complexity of the BS, the BS employs the sub-connected hybrid array with N_t transmit antennas, which is divided into N_{RF} nonoverlapped subarrays, each containing $M = N_t/N_{RF}$ antennas connected to an RF chain through

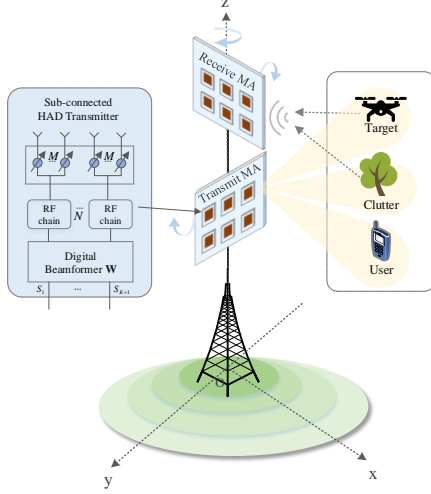


Fig. 1: Illustration of the proposed RA-aided far-field ISAC system.

analog phase shifters. We assume M is an integer for brevity.

A. RA-BS Model

In this paper, we consider an RA-enabled far-field ISAC system. The BS is equipped with N_t transmit antennas and N_r receive antennas, which are respectively fixed on a rotatable transmit antenna plate and a rotatable receive antenna plate, each with an area of D . To avoid coupling effects, we ensure that the distance between any two antennas is always no less than half a wavelength. Without loss of generality, we assume that the antennas lie within the $y - z$ plane of the local Cartesian coordinate system defined by the center of the corresponding plane, and the local positions of the N_t -th transmit antenna and the N_r -th receive antenna can be respectively represented as

$$\mathbf{q}_{n_t}^t = [0, y_{n_t}^t, z_{n_t}^t]^T \in A_t, \quad (1)$$

$$\mathbf{q}_{n_r}^r = [0, y_{n_r}^r, z_{n_r}^r]^T \in A_r, \quad (2)$$

The transmit and receive array are connected to the CPU via rotatable rods embedded with flexible wires, and thus 3D rotations can be adjusted. The 3D rotation can be respectively characterized by

$$\boldsymbol{\varpi}^q = [\alpha^q, \beta^q, \gamma^q]^T, q \in \{t, r\} \quad (3)$$

where $\alpha^q \in [0, 2\pi)$, $\beta^q \in [0, 2\pi)$, $\gamma^q \in [0, 2\pi)$ denote the rotation angles with respect to (w.r.t.) the x -axis, y -axis and z -axis, respectively.

Given $\boldsymbol{\varpi}$, the rotation matrix can be defined as

$$\mathbf{R}(\boldsymbol{\varpi}^q) = \mathbf{R}_{\alpha_q} \mathbf{R}_{\beta_q} \mathbf{R}_{\gamma_q} = \begin{bmatrix} c_{\beta_q} c_{\gamma_q} & c_{\beta_q} s_{\gamma_q} & -s_{\beta_q} \\ s_{\beta_q} s_{\alpha_q} c_{\gamma_q} - c_{\alpha_q} s_{\gamma_q} & s_{\beta_q} s_{\alpha_q} s_{\gamma_q} + c_{\alpha_q} c_{\gamma_q} & c_{\beta_q} s_{\alpha_q} \\ c_{\alpha_q} s_{\beta_q} c_{\gamma_q} + s_{\alpha_q} s_{\gamma_q} & c_{\alpha_q} s_{\beta_q} s_{\gamma_q} - s_{\alpha_q} c_{\gamma_q} & c_{\alpha_q} c_{\beta_q} \end{bmatrix}, \quad (4)$$

with

$$\begin{aligned} \mathbf{R}_{\alpha_q} &= \begin{bmatrix} 1 & 0 & 0 \\ 0 & c_{\alpha_q} & s_{\alpha_q} \\ 0 & -s_{\alpha_q} & c_{\alpha_q} \end{bmatrix}, \\ \mathbf{R}_{\beta_q} &= \begin{bmatrix} c_{\beta_q} & 0 & -s_{\beta_q} \\ 0 & 1 & 0 \\ s_{\beta_q} & 0 & c_{\beta_q} \end{bmatrix}, \\ \mathbf{R}_{\gamma_q} &= \begin{bmatrix} c_{\gamma_q} & s_{\gamma_q} & 0 \\ -s_{\gamma_q} & c_{\gamma_q} & 0 \\ 0 & 0 & 1 \end{bmatrix}, \end{aligned} \quad (5)$$

denoting the rotation matrices w.r.t. each of the x -axis, y -axis and z -axis, respectively, where $c_x = \cos(x)$ and $s_x = \sin(x)$ are defined for notational simplicity. Then the positions of the n_t -th transmit antenna and the n_r -th receive antenna in the global Cartesian coordinate system can be expressed as

$$\mathbf{t}_{n_t} = \mathbf{R}(\boldsymbol{\varpi}^t) \mathbf{q}_{n_t}^t + \mathbf{C}^t, \quad (6)$$

$$\mathbf{r}_{n_r} = \mathbf{R}(\boldsymbol{\varpi}^r) \mathbf{q}_{n_r}^r + \mathbf{C}^r, \quad (7)$$

where \mathbf{C}^t and \mathbf{C}^r denote the centers' positions of transmit plate and receive plate, respectively.

B. Channel Model

Consider a far-field, quasi-static channels, we assume the communication user (CU) and the target are located in the far-field region of the BS. Since the size of each UPA's region is much smaller than the signal propagation distance between the BS and the scatter points and/or receiver, the planar wave is adopted to construct the field-response array model. The pointing vector of the CU/target corresponding to the direction (θ, ϕ) are given by

$$\mathbf{p} = [\sin \theta \cos \phi, \sin \theta \sin \phi, \cos \theta]^T, \quad (8)$$

where $\theta \in [0, \pi]$ and $\phi \in [-\frac{\pi}{2}, \frac{\pi}{2}]$ denote the elevation and azimuth angles, respectively. The difference in signal path distance between the target position \mathbf{p} to the n_t -th transmit antenna and from \mathbf{p} to the n_r -th receive antenna is represented by $\mathbf{p}^T \mathbf{t}_{n_t}(\boldsymbol{\varpi}^t)$ and $\mathbf{p}^T \mathbf{r}_{n_r}(\boldsymbol{\varpi}^r)$, and the corresponding complex form of phase difference are given by $e^{-j\frac{2\pi}{\lambda} \mathbf{p}^T \mathbf{t}_{n_t}(\boldsymbol{\varpi}^t)}$ and $e^{-j\frac{2\pi}{\lambda} \mathbf{p}^T \mathbf{r}_{n_r}(\boldsymbol{\varpi}^r)}$. Taking \mathbf{p} as the reference point, the steer vector of the Tx is

$$\mathbf{a}(\boldsymbol{\varpi}^t) = [e^{-j\frac{2\pi}{\lambda} \mathbf{p}^T \mathbf{t}_1(\boldsymbol{\varpi}^t)}, \dots, e^{-j\frac{2\pi}{\lambda} \mathbf{p}^T \mathbf{t}_{N_t}(\boldsymbol{\varpi}^t)}]^T, \quad (9)$$

where λ denotes the carrier wavelength.

As mentioned in [19], the rotatability of both transmit and receive array must meet some rotation constraints to avoid mutual signal reflections between them. But in this paper, we consider adopting a bistatic setup at the BS, where the Tx and the Rx are separated. Meanwhile, we keep a relatively large distance between the Tx and the Rx to avoid this problem. Therefore, we assume that there is no problem of mutual reflection of signals.

To make the channel model more general, as well as evaluating the influence of array orientation tuning precisely, we take into account the effect of the antenna radiation pattern[10]. According to [28], since the signals are transmitted by different

array elements and received by receiving array elements from distinct angles, there is a significant difference in the pattern of the antennas. The effective antenna pattern is determined by the projection of the array normal to the direction of the signal. Consequently, the channel power gain between the n_t -th transmit antenna and the k -th CU/target \mathbf{p} is given by

$$|h_{n_t,k}^t(\mathbf{p})| = \rho \sqrt{\frac{(\mathbf{p} - \mathbf{t}_{n_t})^T \mathbf{u}^t}{\|\mathbf{p} - \mathbf{t}_{n_t}\|}}, \quad (10)$$

where ρ is the pass loss for the k -th user, $\mathbf{u}^p = \mathbf{R}(\varpi^p) \mathbf{u}_0$ denoting the outward normal vector of the Tx or Rx, $\mathbf{u}_0 = [1, 0, 0]^T$ denotes the original normal vector, $\frac{(\mathbf{p} - \mathbf{t}_{n_t})}{\|\mathbf{p} - \mathbf{t}_{n_t}\|}$ represents the projection of the array normal to the direction of the signal.

Consequently, The communication channel vector $\mathbf{h}_k \in \mathbb{C}^{N_t \times 1}$ between the k -th CU and the Tx can be derived as

$$\mathbf{h}_k = [|h_{n_1,k}^t(\mathbf{p})| [a(\varpi^t)]_1, \dots, |h_{n_t,k}^t(\mathbf{p})| [a(\varpi^t)]_{n_t}]^T \quad (11)$$

and also, the field response vector from the BS to the sensing target/clutters can be written as $\mathbf{G}_\chi \in \mathbb{C}^{N_r \times N_t}$ between the BS and the target is modeled as

$$\mathbf{G}_\chi = \beta_\chi \mathbf{g}_\chi \mathbf{h}_\chi^H, \quad (12)$$

where β_χ represents the target radar cross section (RCS) with $\mathbb{E}\{|\beta_\chi|^2\} = \zeta^2$, $\chi = \{s, 1, \dots, C\}$ representing the target or the clutter, \mathbf{g}_χ and \mathbf{h}_χ represent the channel vector between the transmitter and target and between the receiver and target, respectively.

C. Signal Model

Let $\mathbf{s} \in \mathbb{C}^{(K+1) \times 1}$ be the independent and identically distributed (i.i.d.) signal vector, with $\mathbb{E}(\mathbf{s}\mathbf{s}^H) = \mathbf{I}_{K+1}$, where s_1, \dots, s_K are for K CUs, respectively, and s_{K+1} is dedicated for sensing. Assume that the perfect channel state information (CSI) of communication channels is perfectly known at the BS via a proper channel estimation mechanism. The transmit beamforming matrice is

$$\mathbf{W} = [\underbrace{\mathbf{w}_1, \dots, \mathbf{w}_K}_{\text{for communication and sensing}}, \underbrace{\mathbf{w}_{K+1}}_{\text{dedicated for sensing}}] \in \mathbb{C}^{N_t \times (K+1)}, \quad (13)$$

Then the received signal at the k -th user is then given by

$$\begin{aligned} y_k &= \mathbf{h}_k^H \mathbf{F} \mathbf{W} \mathbf{s} + n_k \\ &= \underbrace{\mathbf{h}_k^H \mathbf{F} \mathbf{w}_k s_k}_{\text{Desired signal}} + \underbrace{\mathbf{h}_k^H \mathbf{F} \mathbf{w}_{k'} s_{k'}}_{\text{Interference}} + n_k, \end{aligned} \quad (14)$$

where $\mathbf{w}_k \in \mathbb{C}^{N_t \times 1}$ denoted the digital transmit beamforming vector for the user $k \in \mathcal{K}$, $\mathbf{F} \in \mathbb{C}^{N_t \times N_{RF}}$ is the analog precoding matrix, and $n_k \sim \mathcal{CN}(0, \sigma_k^2)$ is zero-mean additive white Gaussian noise (AWGN) with noise power σ_k^2 . With this sub-connected structure, the analog precoder matrix \mathbf{F} is given by

$$\mathbf{F} = \text{Bdiag}(\mathbf{f}_1, \mathbf{f}_2, \dots, \mathbf{f}_{N_{RF}}) \in \mathbb{C}^{N_t \times N_{RF}}, \quad (15)$$

where $\mathbf{f}_i \in \mathbb{C}^{M \times 1}, i = 1, 2, \dots, N_{RF}$, is an $M = N_t / N_{RF}$ dimensional vector with each element being constant modulus

value, i.e., $|\mathbf{f}_i(j)| = 1, j = 1, \dots, M$. Hence, the received data rate of user k can be obtained as

$$R_k = \log_2(1 + \text{SINR}_k), \quad (16)$$

where

$$\text{SINR}_k = \frac{|\mathbf{h}_k^H \mathbf{F} \mathbf{w}_k|}{\sum_{j=1, j \neq k}^{K+1} |\mathbf{h}_k^H \mathbf{F} \mathbf{w}_j|^2 + \sigma_k^2}, \quad (17)$$

As for sensing, The BS applies the receive beamformer, $\mathbf{u} \in \mathbb{C}^{N_r \times 1}$ to capture the reflected signal of target s . The received signal at the BS can be expressed as

$$y_s = \underbrace{\zeta_s \mathbf{u}^H \mathbf{G}_s \mathbf{F} \mathbf{W} \mathbf{s}}_{\text{Target reflection}} + \underbrace{\sum_{c=1}^C \zeta_c \mathbf{u}^H \mathbf{G}_c \mathbf{F} \mathbf{W} \mathbf{s}}_{\text{Clutters reflection}} + n_s, \quad (18)$$

where $n_s \sim \mathcal{CN}(0, \sigma_s^2)$ denotes the AWGN for radar link. ζ_s and ζ_c are complex coefficients including the radar cross section (RCS) of the target/ clutter, respectively. Additionally, \mathbf{G}_s and \mathbf{G}_c denote the array response vectors between the BS and the target/clutter, respectively.

We assume point-like target and clutters, since the sizes of the target and the clutters are sufficiently small compared to the distances of the reflecting paths. Thus, the radar signal-to-clutter-plus-noise-ratio (SCNR) at the RX can be expressed as

$$\text{SCNR} = \frac{||\zeta_s \mathbf{u}^H \mathbf{G}_s \mathbf{F} \mathbf{W} \mathbf{s}||^2}{||\sum_{c=1}^C \zeta_c \mathbf{u}^H \mathbf{G}_c \mathbf{F} \mathbf{W} \mathbf{s}||^2 + \sigma_s^2}, \quad (19)$$

For point target detection in MIMO radar systems, to quantify how much information can be extracted with a given sensing signal, we can use the sensing mutual information (MI) per unit time [29] [30]. It is defined as the MI between the received signal at the BS and the target response, conditioned on the transmitted signal. Specifically, the BS has knowledge of both the receive beamformer \mathbf{u} and the transmitted ISAC signal \mathbf{x} , the conditional sensing MI between the received echo and the target response (or the sensing rate) as [22]

$$R_s = I(y_s; \zeta_s \mathbf{G}_s | \mathbf{u}, \mathbf{x}) = \log_2(1 + \text{SCNR}) \quad (20)$$

where $\mathbf{x} = \mathbf{F} \mathbf{W} \mathbf{s}$ denotes the transmitted signal.

D. Problem Formulation

To balance the communication and sensing performance, We aim to maximize the weighted sum of communication rate and sensing MI in (16) and (20). The optimization problem is formulated as

$$\max_{\mathbf{u}, \mathbf{F}, \mathbf{W}, \Lambda} \mathcal{G}(\mathbf{u}, \mathbf{F}, \mathbf{W}, \Lambda) = \varpi_c \sum_{k=1}^K R_k + \varpi_s R_s \quad (21a)$$

$$\text{s.t. } \|\mathbf{u}\|_2^2 = 1, \quad (21b)$$

$$\|\mathbf{F} \mathbf{W}\|_F^2 \leq P_{max}, \quad (21c)$$

$$\mathbf{F} \in \mathcal{A}_F, \quad (21d)$$

where the weighting factors ϖ_s and ϖ_c control the priority of communication and sensing satisfy $\varpi_s + \varpi_c = 1$, $\Lambda = [\alpha^t, \beta^t, \gamma^t, \alpha^r, \beta^r, \gamma^r]$ represent the sets of rotation angles for the transmit and receive planes. Constraint (21b) normalize

the receive beamformer. Constraint (21c) denotes the transmit power should not exceed the maximum limits. Constraint (21d) corresponds to the sub-connected structure, i.e., the analog \mathbf{F} belongs to a set of block matrices \mathcal{A}_p , where each block is an M dimension vector with unit modulus elements. Due to the non-concave/non-convex objective function/constraints, problem (21) is difficult to solve. Specifically, in contrast to the existing FPA-based hybrid beamforming designs, the position change brought about by the rotatability of the transmitting and receiving antennas makes the variable coupling of the numerator and denominator in the achievable rates of users and targets more complex, thus posing further challenges. Moreover, Since the resource allocation needs to meet the different demands of the two functions, the trade-off between communication and sensing needs to be investigated.

It is worth mentioning that, for simplicity, we focus on a single target in this paper. Since our proposed scheme can treat the echoes from other targets as radar interference in the denominator of (19), the proposed algorithm can be similarly adapted to address the multi-target problem.

III. PROPOSED ALGORITHM

In this section, we propose an efficient algorithm for solving problem (21) by optimizing the transmit digital beamformer, transmit analog beamformer, receive beamformer, the rotation angles of the transmitting and receiving plate. The problem is non-convex due to its objective function and coupling variables. To tackle this problem, we propose an alternating optimization (AO)-based algorithm where we update each variable with fixed values of the other variables obtained from the last iteration.

Given the mutual coupling between digital beamformer and analog beamformer in the objective and constraint (21c), it is generally difficult to optimize these two parameters simultaneously. Moreover, the non-convex SINR, SCNR and unit-modulus constraints make the problem even more challenging. A typical method is to first design the fully-digital beamformer and then approach the fully-digital one via hybrid beamformer design [9] [31]. However, the obtained solution based on such a two-stage method cannot guarantee the original constraints to be satisfied. Therefore, we propose to directly optimize the digital beamformer and analog beamformer based on the principle of alternating optimization. For the variables \mathbf{F} , \mathbf{W} , Λ , we employ the fractional programming (FP) approach

[32]. We introduce auxiliary variables $\boldsymbol{\mu} = [\mu_1, \dots, \mu_{K+1}]$, $\boldsymbol{\xi}^c = [\xi_1^c, \dots, \xi_K^c]^T$ and $\boldsymbol{\xi}^s = [\xi_1^s, \dots, \xi_{K+1}^s]^T$ to transform the (21a) into an equivalent convex form (22). Based on the AO framework, The problem (21) can be decomposed as five subproblems. The details of the proposed algorithms are presented below.

A. Receive Beamforming Optimization

Given $\{\mathbf{F}, \mathbf{W}, \Lambda\}$, the optimization of \mathbf{u} only affect the SCNR (19). Therefore, maximizing the WSR, i.e., objective value (21a), is equivalent to maximizing SCNR (19). Hence, we formulate the subproblem for \mathbf{u}

$$\begin{aligned} \mathcal{SP}_1 : \max_{\mathbf{u}} \quad & \text{SCNR} \\ \text{s.t.} \quad & (21b). \end{aligned} \quad (23a)$$

Based on the expressed in (23), it is found that the maximization of SCNR belongs to the problem of generalized Rayleigh quotient. By applying **Proposition 1**, the optimal closed-form solution can be obtained.

Proposition 1. The optimal solutions of problem (23) is given by

$$\mathbf{u}^* = \frac{\left(\sum_{c=1}^C \tilde{\mathbf{f}}_c \tilde{\mathbf{f}}_c^H + \sigma_s^2 \mathbf{I}_{N_r} \right)^{-1} \mathbf{b}_s}{\left\| \left(\sum_{c=1}^C \tilde{\mathbf{f}}_c \tilde{\mathbf{f}}_c^H + \sigma_s^2 \mathbf{I}_{N_r} \right)^{-1} \mathbf{b}_s \right\|_2}, \quad (24)$$

where $\mathbf{b}_s = \mathbf{G}_s (\sum_{k=1}^{K+1} \mathbf{F} \mathbf{w}_k) \in \mathbb{C}^{N_r \times 1}$ and $\tilde{\mathbf{f}}_c = \zeta_c \mathbf{G}_c \mathbf{F} \mathbf{W} \in \mathbb{C}^{N_r \times (K+1)}$.

Proof. we rewrite the numerator part of Formula (20) as

$$\begin{aligned} |\zeta_s|^2 \mathbf{u}^H \mathbf{G}_s \tilde{\mathbf{A}} \mathbf{G}_s^H \mathbf{u} \\ = |\zeta_s|^2 \mathbf{u}^H \mathbf{g}_s \mathbf{h}_s^H \tilde{\mathbf{A}} \mathbf{h}_s \mathbf{g}_s^H \mathbf{u} \\ = |\zeta_s|^2 \mathbf{h}_s^H \tilde{\mathbf{A}} \mathbf{h}_s \mathbf{u}^H \mathbf{g}_s \mathbf{g}_s^H \mathbf{u}. \end{aligned} \quad (25)$$

Since $|\zeta_s|^2 \mathbf{h}_s^H \tilde{\mathbf{A}} \mathbf{h}_s$ is non-negative and independent of the receive beamformer \mathbf{u} , based on the research results in Reference [33], we apply the generalized Rayleigh quotient to maximize problem (23) and arrive at the optimal solution \mathbf{u}^* , which is a minimal mean-square error (MMSE) filter. \square

$$\begin{aligned} \tilde{\mathcal{G}}(\mathbf{F}, \mathbf{W}, \boldsymbol{\mu}, \boldsymbol{\xi}^c, \boldsymbol{\xi}^s, \Lambda) = & \varpi_c \sum_{k=1}^K \log(1 + \mu_k) + \varpi_s \log(1 + \mu_{K+1}) - \varpi_c \sum_{k=1}^K \mu_k - \varpi_s \mu_{K+1} \\ & + \varpi_c \sum_{k=1}^K \left(2\sqrt{1 + \mu_k} \operatorname{Re}\{\xi_k^c \mathbf{h}_k^H(\Lambda) \mathbf{F} \mathbf{w}_k\} - |\xi_k^c|^2 \left(\sum_{j=1}^{K+1} |\mathbf{h}_k^H(\Lambda) \mathbf{F} \mathbf{w}_j|^2 + \sigma_k^2 \right) \right) \\ & + \varpi_s \left(2\sqrt{1 + \mu_{K+1}} \operatorname{Re}\{\zeta_s \mathbf{u}^H \mathbf{G}_s(\Lambda) \mathbf{F} \mathbf{W} \boldsymbol{\xi}^s\} \right. \\ & \left. - \|\boldsymbol{\xi}^s\|^2 \left(\sum_{c=1}^C \|\zeta_c \mathbf{u}^H \mathbf{G}_c(\Lambda) \mathbf{F} \mathbf{W}\|^2 + \|\zeta_s \mathbf{u}^H \mathbf{G}_s(\Lambda) \mathbf{F} \mathbf{W}\|^2 + \sigma_s^2 \right) \right) \end{aligned} \quad (22)$$

B. Transmit Digital Beamforming Optimization

Given $\{\mathbf{u}, \mathbf{F}, \mathbf{\Lambda}, \boldsymbol{\mu}, \boldsymbol{\xi}^s, \boldsymbol{\xi}^c\}$, we optimize the digital beamformer \mathbf{W} . To decouple the product of \mathbf{F} and \mathbf{W} in the original power constraint (21c), we reformulate the power constraint in accordance with the special analog precoding structure as follows[1]:

$$\|\mathbf{F}\mathbf{W}\|_F^2 = \frac{N_t}{N_{RF}} \|\mathbf{W}\|_F^2 = M \|\mathbf{W}\|_F^2, \quad (26)$$

Thus, The subproblem of transmit digital beamformer design is formulated as

$$\max_{\mathbf{W}} \tilde{\mathcal{G}}(\mathbf{u}, \mathbf{F}, \mathbf{\Lambda}, \boldsymbol{\mu}, \boldsymbol{\xi}^s, \boldsymbol{\xi}^c) \quad (27a)$$

$$\text{s.t. } \|\mathbf{W}\|_F^2 \leq \frac{P_{\max}}{M}. \quad (27b)$$

Since $\tilde{\mathcal{G}}$ is a convex function with respect to \mathbf{W} , we can employ the Lagrange dual method to obtain the closed-form expression of \mathbf{W} . The Lagrangian function is defined as

$$\begin{aligned} \mathcal{L}(\mathbf{W}, \lambda) = & -\tilde{\mathcal{G}}(\mathbf{W}|\mathbf{u}, \mathbf{F}, \mathbf{\Lambda}, \boldsymbol{\mu}, \boldsymbol{\xi}^s, \boldsymbol{\xi}^c) \\ & + \lambda(\|\mathbf{W}\|_F^2 - \frac{P_{\max}}{M}), \end{aligned} \quad (28)$$

where $\lambda \geq 0$ is the Lagrange multiplier corresponding to the power constraint. The KKT conditions are used to solve the dual problem as

$$\frac{\partial \mathcal{L}(\mathbf{W}, \lambda)}{\partial \mathbf{W}} = \mathbf{0}, \quad (29)$$

$$\|\mathbf{W}\|_F^2 - \frac{P_{\max}}{M} \leq 0, \quad (30)$$

$$\lambda \geq 0, \quad (31)$$

$$\lambda \left(\|\mathbf{W}\|_F^2 - \frac{P_{\max}}{M} \right) = 0. \quad (32)$$

The closed-form expression of \mathbf{W} can be obtained by solving (29), which is

$$\mathbf{w}_k(\lambda) = \left((\mathbf{\Lambda}_k^T + \lambda \mathbf{I}_{N_{RF}})^{-1} \right)^* \boldsymbol{\varphi}_k, \quad \forall k \in \{1, \dots, K+1\}, \quad (33)$$

where

$$\begin{aligned} \mathbf{\Lambda}_k = & \varpi_c \sum_{k=1}^K |\xi_k^c|^2 (\mathbf{h}_k^H \mathbf{F})^H (\mathbf{h}_k^H \mathbf{F}) \\ & + \varpi_s \|\boldsymbol{\xi}^s\|^2 \left\{ |\zeta_s|^2 (\mathbf{u}^H \mathbf{G}_s \mathbf{F})^H (\mathbf{u}^H \mathbf{G}_s \mathbf{F}) \right. \\ & \left. + \sum_{c=1}^C |\zeta_c|^2 (\mathbf{u}^H \mathbf{G}_c \mathbf{F})^H (\mathbf{u}^H \mathbf{G}_c \mathbf{F}) \right\}, \end{aligned} \quad (34)$$

$$\begin{aligned} \boldsymbol{\varphi}_k = & \varpi_c \sqrt{1 + \mu_k} (\xi_k^c \mathbf{h}_k^H \mathbf{F})^H + \varpi_s \sqrt{1 + \mu_{K+1}} \\ & \times (\zeta_s \xi_k^s \mathbf{u}^H \mathbf{G}_s \mathbf{F})^H, \quad \text{for } k \in \{1, \dots, K\}, \end{aligned} \quad (35)$$

$$\boldsymbol{\varphi}_{K+1} = \varpi_s \sqrt{1 + \mu_{K+1}} (\zeta_s \xi_{K+1}^s \mathbf{u}^H \mathbf{G}_s \mathbf{F})^H. \quad (36)$$

We employ a bisection method to select an appropriate dual variable λ to satisfy the complementary slackness condition (32). If the peimal feasibility satisfied $\|\mathbf{W}^*\|_F^2 \leq \frac{P_{\max}}{M}$, $\lambda = 0$. otherwise, λ needs to be decided to satisfy

Algorithm 1 Bisection Method for Searching Dual Variable λ

```

1: Initialize upper and lower bound  $\lambda_{\max}$ ,  $\lambda_{\min}$ , tolerance  $\varepsilon$  and iteration index  $l = 0$ .
2: repeat
3:   Compute  $\lambda^{(l)} = (\lambda_{\min} + \lambda_{\max})/2$ .
4:   Replace  $\lambda^{(l)}$  in  $\mathbf{W}(\lambda)$  and compute  $h(\lambda^{(l)})$ .
5:   if  $h(\lambda^{(l)}) > 0$  then
6:     Set  $\lambda_{\min} = \lambda^{(l)}$ .
7:   else
8:     Set  $\lambda_{\max} = \lambda^{(l)}$ .
9:   end if
10:  Set iteration index  $l = l + 1$ .
11: until  $|h(\lambda^{(l)})| \leq \varepsilon$ 
12: Output: optimal dual variable  $\lambda^*$ .

```

$$h(\lambda) = \|\mathbf{W}(\lambda)\|_F^2 - \frac{P_{\max}}{M} \leq \varepsilon. \quad (37)$$

The bisection method can be adopted to find the solution of λ [34], which is summarized in **Algorithm 1**.

C. Transmit Analog Beamforming Optimization

With given $\{\mathbf{u}, \mathbf{W}, \mathbf{\Lambda}, \boldsymbol{\mu}, \boldsymbol{\xi}^s, \boldsymbol{\xi}^c\}$, we optimize the analog beamformer \mathbf{F} . The subproblem of analog beamformer design is formulated as

$$\begin{aligned} \max_{\mathbf{F}} & \tilde{\mathcal{G}}(\mathbf{u}, \mathbf{W}, \mathbf{\Lambda}, \boldsymbol{\mu}, \boldsymbol{\xi}^s, \boldsymbol{\xi}^c) \\ \text{s.t. } & (21d). \end{aligned} \quad (38a)$$

Note that the analog beamformer \mathbf{F} is block diagonal, i.e., most of its element are zeros. To reduce the computational complexity, we extract the non-zero elements of \mathbf{F} as

$$\mathbf{d} = [\mathbf{f}_1^T, \dots, \mathbf{f}_{N_{RF}}^T]^T \in \mathbb{C}^{N_t \times 1}. \quad (39)$$

The singular value decomposition (SVD) of \mathbf{W} with a rank of R is

$$\mathbf{W} = \sum_{r=1}^R \rho_r \mathbf{u}_r \mathbf{v}_r^H, \quad (40)$$

where ρ_r , \mathbf{u}_r and \mathbf{v}_r are the r -th eigenvalue, left and right singular matrix, respectively. Define $\tilde{\mathbf{u}}_r = \sqrt{\rho_r} \mathbf{u}_r$, $\tilde{\mathbf{v}}_r = \sqrt{\rho_r} \mathbf{v}_r$ and $\tilde{\mathbf{V}}_j = \tilde{\mathbf{v}}_j^H \tilde{\mathbf{v}}_j$. Then by applying the matrix transformation, the problem (38) can be recast as

$$\begin{aligned} \max_{\mathbf{d}} \quad & \tilde{\mathcal{P}} = \varpi_c \sum_{k=1}^K \left(2\Re\{\tilde{\beta}_k^H \mathbf{d}\} - |\xi_k^c|^2 \sum_{j=1}^{K+1} |\tilde{\mathbf{h}}_{k,j}^H \mathbf{d}|^2 \right) \\ & + \varpi_s \left(2\Re\{\tilde{\beta}_s^H \mathbf{d}\} - \|\boldsymbol{\xi}^s\|^2 \left(\sum_{c=1}^C \left\| \sum_{r=1}^R \mathbf{u}^H \tilde{\mathbf{G}}_{c,r} \mathbf{d} \tilde{\mathbf{v}}_r^H \right\|^2 \right. \right. \\ & \left. \left. + \left\| \sum_{r=1}^R \mathbf{u}^H \tilde{\mathbf{G}}_{s,r} \mathbf{d} \tilde{\mathbf{v}}_r^H \right\|^2 \right) \right) + \text{const}(\boldsymbol{\mu}) \end{aligned} \quad (41a)$$

$$\text{s.t. } |[\mathbf{d}]_n| = 1, \quad \forall n = 1, 2, \dots, N_t, \quad (41b)$$

where $\text{const}(\boldsymbol{\mu})$ is a constant term when $\boldsymbol{\mu}$ is fixed, $\tilde{\mathbf{h}}_{k,j}^H = \mathbf{h}_k^H (\text{diag}(\mathbf{w}_j) \otimes \mathbf{I}_M)$, $\tilde{\beta}_k^H = \sqrt{1 + \mu_k} \xi_k^{c*} \tilde{\mathbf{h}}_{k,k}^H$,

$\tilde{\beta}_s^H = \sqrt{1 + \mu_{K+1}} \zeta_s^* \mathbf{u}^H \mathbf{G}_s (\text{diag}(\mathbf{W} \boldsymbol{\xi}_s) \otimes \mathbf{I}_M)$ and $\tilde{\mathbf{G}}_{c,r} = \zeta_c \mathbf{G}_c (\text{diag}(\tilde{\mathbf{u}}_r) \otimes \mathbf{I}_M)$. Problem (41) is subject to the unit modulus constraint (41b). A conventional approach is to adopt Riemannian manifold optimization and solve it using the conjugate gradient descent method. However, this method suffers from low efficiency and unstable algorithm performance. To address the problem (41), we introduce the continuous variable ϕ . Thus the subproblem (41a) is formulated as

$$\max \tilde{\mathcal{P}} - \eta \|\phi - \mathbf{d}\|_2^2, \quad (42)$$

where $\eta > 0$ is the penalty parameter. Based on the penalty method, problem (41) can be solved via updating \mathbf{d} and ϕ iteratively. With given \mathbf{d} , the optimal solution of ϕ is

$$\phi^* = [\tilde{\mathbf{E}}]^{-1} \tilde{\beta} \quad (43)$$

where $\tilde{\mathbf{E}} = \varpi_c \sum_{k=1}^K |\xi_k^c|^2 \sum_{j=1}^{K+1} (\tilde{\mathbf{h}}_{k,j} \tilde{\mathbf{h}}_{k,j}^H) + \varpi_s \|\boldsymbol{\xi}^s\|^2 (\sum_{c=1}^C \sum_{r=1}^R \tilde{V}_j \tilde{\mathbf{G}}_{c,r}^H \tilde{\mathbf{G}}_{c,r} + \sum_{r=1}^R \tilde{V}_j \tilde{\mathbf{G}}_{s,r}^H \tilde{\mathbf{G}}_{s,r}) + \eta \mathbf{I}_M$, $\tilde{\beta} = \varpi_c \sum_{k=1}^K \tilde{\beta}_k + \varpi_s \tilde{\beta}_s + \eta \mathbf{d}$. With given ϕ , the optimization of \mathbf{d} can be obtained from (41) as

$$\begin{aligned} \min_{\mathbf{d}} \|\phi - \mathbf{d}\|_2^2 \\ \text{s.t. (41b).} \end{aligned} \quad (44a)$$

The optimal phase of \mathbf{d} is given by

$$\arg\{\mathbf{d}\} = \arg\{\phi\}, \quad (45)$$

Finally, by performing a simple matrix transformation on \mathbf{d} , the optimized variable \mathbf{F} can be obtained.

D. Auxiliary Variables Optimization

Since $\tilde{\mathcal{G}}(\boldsymbol{\xi}_c, \boldsymbol{\xi}_s, \boldsymbol{\mu} | \mathbf{u}, \mathbf{F}, \mathbf{W}, \boldsymbol{\Lambda})$ is concave w.r.t. auxiliary variables $\boldsymbol{\xi}_c, \boldsymbol{\xi}_s$ for quadratic transform and auxiliary variable $\boldsymbol{\mu}$ for lagrangian dual transform. With given fixed other parameters, we can obtained the closed-form solutions of $\boldsymbol{\xi}_c, \boldsymbol{\xi}_s$ and $\boldsymbol{\mu}$ by setting the partial derivatives to zeros, i.e., $\frac{\partial \tilde{\mathcal{G}}(\boldsymbol{\xi}_c | \mathbf{u}, \mathbf{F}, \mathbf{W}, \boldsymbol{\Lambda}, \boldsymbol{\xi}_s, \boldsymbol{\mu})}{\partial \boldsymbol{\xi}_c} = 0$, $\frac{\partial \tilde{\mathcal{G}}(\boldsymbol{\xi}_s | \mathbf{u}, \mathbf{F}, \mathbf{W}, \boldsymbol{\Lambda}, \boldsymbol{\xi}_c, \boldsymbol{\mu})}{\partial \boldsymbol{\xi}_s} = 0$ and $\frac{\partial \tilde{\mathcal{G}}(\boldsymbol{\mu} | \mathbf{u}, \mathbf{F}, \mathbf{W}, \boldsymbol{\Lambda}, \boldsymbol{\xi}_c, \boldsymbol{\xi}_s)}{\partial \boldsymbol{\mu}} = 0$, respectively. Thus, we can derive the closed-form solutions for the auxiliary variables $\boldsymbol{\xi}_c$ and $\boldsymbol{\xi}_s$ related to the quadratic transformation as follows

$$\xi_k^c = \frac{\sqrt{1 + \mu_k} (\mathbf{h}_k^H \mathbf{F} \mathbf{w}_k)^H}{\sum_{j=1}^{K+1} |\mathbf{h}_k^H \mathbf{F} \mathbf{w}_j|^2 + \sigma_k^2}, \forall k = 1, \dots, K, \quad (46)$$

$$\boldsymbol{\xi}^s = \frac{\sqrt{1 + \mu_{K+1}} (\zeta_s \mathbf{u}^H \mathbf{G}_s \mathbf{F} \mathbf{W})^H}{\sum_{c=1}^C \|\zeta_c \mathbf{u}^H \mathbf{G}_c \mathbf{F} \mathbf{W}\|^2 + \|\zeta_s \mathbf{u}^H \mathbf{G}_s \mathbf{F} \mathbf{W}\|^2 + \sigma_s^2}. \quad (47)$$

Similarly, we can derive the closed-form solution for the auxiliary variable $\boldsymbol{\mu}$ related to the lagrangian dual transform, which gives

$$\mu_k = \frac{|\mathbf{h}_k^H \mathbf{F} \mathbf{w}_k|^2}{\sum_{j \neq k}^{K+1} |\mathbf{h}_k^H \mathbf{F} \mathbf{w}_j|^2 + \sigma_k^2}, \forall k = 1, \dots, K, \quad (48)$$

$$\mu_{K+1} = \frac{\|\zeta_s \mathbf{u}^H \mathbf{G}_s \mathbf{F} \mathbf{W}\|^2}{\sum_{c=1}^C \|\zeta_c \mathbf{u}^H \mathbf{G}_c \mathbf{F} \mathbf{W}\|^2 + \sigma_s^2}, \quad (49)$$

E. Antenna Rotation Optimization

In this subsection, we optimize the antenna rotation angle $\boldsymbol{\Lambda}$ with any given other variables. $\boldsymbol{\Lambda} = [\alpha^t, \beta^t, \gamma^t, \alpha^r, \beta^r, \gamma^r]$ is the set of rotation angles of the transmitting and receiving plates. To optimize $\boldsymbol{\Lambda}$, a feasible approach is to adopt an alternating optimization strategy, optimizing each element one by one until all elements in $\boldsymbol{\Lambda}$ are optimized. The transmit antenna rotation optimization and the receive antenna rotation optimization have similar mathematical formulations. For simplicity, we will focus on the optimization of the transmitting antenna rotation, and let $\boldsymbol{\Lambda}$ contain only one variable among α_t, β_t and γ_t , with this variable denoted as $\tilde{\Lambda}$. The subproblem of antenna rotation design is formulated as

$$\max_{\tilde{\Lambda}} \tilde{\mathcal{G}}(\mathbf{u}, \mathbf{W}, \mathbf{F}, \boldsymbol{\mu}, \boldsymbol{\xi}^s, \boldsymbol{\xi}^c). \quad (50)$$

Problem (50) is difficult to solve directly because of its non-convexity. Here, we use $\tilde{\mathcal{G}}$ to replace $\tilde{\mathcal{G}}(\mathbf{u}, \mathbf{W}, \mathbf{F}, \boldsymbol{\mu}, \boldsymbol{\xi}^s, \boldsymbol{\xi}^c)$ for simplicity. It is noted that $\tilde{\mathcal{G}}$ is differentiable across the entire feasible region, so we utilized the gradient ascent (GA) method to find a local stationary point efficiently. Derivative $\frac{\partial \tilde{\mathcal{G}}}{\partial \tilde{\Lambda}}$ can be rewritten as

$$\begin{aligned} \frac{\partial \tilde{\mathcal{G}}(\tilde{\Lambda})}{\partial \tilde{\Lambda}} &= \varpi_c \sum_{k=1}^K \sqrt{1 + \mu_k} \frac{\partial \mathcal{F}_{1,k}(\tilde{\Lambda})}{\partial \tilde{\Lambda}} \\ &- \varpi_c \sum_{k=1}^K |\xi_k^c|^2 \sum_{j=1}^{K+1} \frac{\partial \mathcal{F}_{2,k,j}(\tilde{\Lambda})}{\partial \tilde{\Lambda}} + \varpi_s \sqrt{1 + \mu_{K+1}} \frac{\partial \mathcal{F}_3(\tilde{\Lambda})}{\partial \tilde{\Lambda}} \\ &- \varpi_s \|\boldsymbol{\xi}^s\|^2 \sum_{c=1}^C \frac{\partial \mathcal{F}_{4,c}(\tilde{\Lambda})}{\partial \tilde{\Lambda}} - \varpi_s \|\boldsymbol{\xi}^s\|^2 \frac{\partial \mathcal{F}_5(\tilde{\Lambda})}{\partial \tilde{\Lambda}}, \end{aligned} \quad (51)$$

where

$$\mathcal{F}_{1,k}(\tilde{\Lambda}) = 2\Re \left\{ \xi_k^c \mathbf{h}_k^H(\tilde{\Lambda}) \mathbf{F} \mathbf{w}_k \right\}, \quad (52)$$

$$\mathcal{F}_{2,k,j}(\tilde{\Lambda}) = |\mathbf{h}_k^H(\tilde{\Lambda}) \mathbf{F} \mathbf{w}_j|^2, \quad (53)$$

$$\mathcal{F}_3(\tilde{\Lambda}) = 2\Re \left\{ \zeta_s \mathbf{u}^H \mathbf{G}_s(\tilde{\Lambda}) \mathbf{F} \mathbf{W} \boldsymbol{\xi}^s \right\}, \quad (54)$$

$$\mathcal{F}_{4,c}(\tilde{\Lambda}) = \|\zeta_c \mathbf{u}^H \mathbf{G}_c(\tilde{\Lambda}) \mathbf{F} \mathbf{W}\|^2, \quad (55)$$

$$\mathcal{F}_5(\tilde{\Lambda}) = \|\zeta_s \mathbf{u}^H \mathbf{G}_s(\tilde{\Lambda}) \mathbf{F} \mathbf{W}\|^2. \quad (56)$$

Define $\mathbf{D}_{k,n_t} = \mathbf{P}_k - \mathbf{t}_{n_t}$, $\bar{\mathbf{R}}_v$ denotes the derivative of the rotation matrix \mathbf{R} with respect v , where $v \in \{\alpha, \beta, \gamma\}$. The partial derivatives w.r.t. $\tilde{\Lambda}$ are derived as (57)–(62).

However, the performance of the GA is highly dependent on the step size, i.e., an excessively large step size may cause oscillations in the iteration process or even failure to converge; an excessively small step size, on the other hand, may lead the algorithm to fall into a local optimum prematurely, significantly reducing the optimization efficiency. Meanwhile, the optimization results of this method are equally sensitive to the choice of initial points, i.e., if the initial point falls within the attraction domain of a local optimal solution, the algorithm will directly converge to that local optimum and struggle to escape to a better solution.

To address these shortcomings, we propose an improved GA method. We first determine a relatively optimal initial point for GA through a preliminary search, and then employ

an adaptive step size strategy for iterative searching until a feasible point is found or the convergence condition is met. Based on the above discussions, we propose an improved GA approach to solve the problem (50).

Initially, we set a discrete point set \mathcal{K} with K_r uniformly distributed points in the feasible region \mathcal{N} . Therefore, we can find an optimal initial $\tilde{\Lambda}$ that maximizes $\tilde{\mathcal{G}}$ as

$$\tilde{\Lambda}^{(0)} = \arg \max_{k_r \in \mathcal{K}} \tilde{\mathcal{G}}, \quad k_r \in \{1, \dots, K_r\}. \quad (63)$$

To ensure that in each iteration of the algorithm, the parameter is updated to a feasible point and remains within the feasible region, the update rule for $\tilde{\Lambda}^{(t+1)}$ is defined as:

$$\tilde{\Lambda}^{(t+1)} = \begin{cases} \tilde{\Lambda} \bmod 2\pi, & \text{if } \tilde{\mathcal{G}}(\tilde{\Lambda}) \geq \tilde{\mathcal{G}}(\tilde{\Lambda}^{(t)}), \\ \tilde{\Lambda}^{(t)}, & \text{otherwise,} \end{cases} \quad (64)$$

where $\tilde{\Lambda} = \tilde{\Lambda}^{(t)} + \kappa \nabla \tilde{\mathcal{G}}(\tilde{\Lambda}^{(t)})$ with κ being the step size for GA in each iteration, (t) indicates the value obtained from the last iteration in the inner loop for rotation angle optimization. Since $\tilde{\Lambda}$ represents a rotation angle with a period of 2π , the operation $\tilde{\Lambda} \bmod 2\pi$ ensure it stays within $[0, 2\pi)$. Given that GA method is particularly sensitive to step-size selection, although using a fixed step size is relatively simple to implement, it can easily prevent the optimization results from converging. Thus, we initialize κ with a large positive number. Whenever $\tilde{\mathcal{G}}(\tilde{\Lambda}) \geq \tilde{\mathcal{G}}(\tilde{\Lambda}^{(t)})$, we iteratively update κ as $\kappa \leftarrow \frac{\kappa}{2}$ until κ is reduced to κ_{min} . This step size reduction ensures sufficient refinement of κ while preventing excessive oscillations in the iterations. It can be observed that the sequence $\{\tilde{\mathcal{G}}(\tilde{\Lambda}^{(t)})\}$ keeps non-decreasing based on update guidelines (64), leading to the convergence of the sequence.

In this subsection, we focus on the case where Λ contains only one parameter. However, our method can be readily extended to scenarios involving multiple parameters. Specifically, it suffices to gradually optimize each variable in Λ using alternating iteration approach until the optimal Λ^* is obtained.

Algorithm 2 Proposed Alternating Optimization Algorithm for Flexible Beamforming Design

```

1: Initialize:  $\mathbf{u}^{(0)}, \mathbf{F}^{(0)}, \mathbf{W}^{(0)}, \boldsymbol{\xi}_c^{(0)}, \boldsymbol{\xi}_s^{(0)}, \mu^{(0)}, \boldsymbol{\Lambda}^{(0)}, \kappa^{(0)}$ , the
   iteration index  $t = 0$  and the maximal iteration number  $I_{AO}$ .
2: repeat
3:   Obtain  $\mathbf{W}^{(t)}$  via (27)
4:   Obtain  $\mathbf{F}^{(t)}$  via (41) and (44)
5:   Update initial points  $\tilde{\Lambda}^{(0)}$  via (63)
6:   Calculate the gradient  $\nabla_{\tilde{\Lambda}} \tilde{\mathcal{G}}(\tilde{\Lambda}^{(t)})$  via (51)
7:   Initialize the step size  $\kappa = \kappa^{(0)}$ 
8:   for each  $\tilde{\Lambda}$  in  $\boldsymbol{\Lambda}$  do
9:     repeat
10:      Compute  $\hat{\Lambda} = \tilde{\Lambda}^{(t)} + \kappa \nabla \tilde{\mathcal{G}}(\tilde{\Lambda}^{(t)})$ 
11:      Shrink the step size  $\kappa \leftarrow \frac{\kappa}{2}$ 
12:      Update  $\tilde{\Lambda}^{(t+1)}$  according to (64)
13:    until Converges
14:   end for
15:   Obtain  $\mathbf{u}^{(t)}$  via (24)
16:   Update  $\mu^{(t)}$  via (48) and (49)
17:   Update  $\boldsymbol{\xi}_c^{(t)}$  and  $\boldsymbol{\xi}_s^{(t)}$  via (46) and (47), respectively
18:   Update  $t = t + 1$ 
19: until The value of the objective function (21) converges
   or the maximum iteration number  $I_{AO}$  is reached.
20: Output:  $\mathbf{u}^*, \mathbf{W}^*, \mathbf{F}^*, \boldsymbol{\Lambda}^*$ 

```

F. Overall Algorithm

Based on the algorithms presented above, the detailed overall alternating optimization algorithm for solving the original problem (21) in **Algorithm 2**.

The total complexity of **Algorithm 2** stems from the solving the variables $\{\mathbf{u}, \mathbf{W}, \mathbf{F}, \boldsymbol{\Lambda}, \mu, \boldsymbol{\xi}_c, \boldsymbol{\xi}_s\}$. The computational complexity for calculating receive beamformer \mathbf{u} is $\mathcal{O}(N_r^3)$ due to the matrix inversion in (24). Similarly, The computational

$$\frac{\partial [\mathbf{h}_k(\tilde{\Lambda})]_{n_t}}{\partial \tilde{\Lambda}} = \frac{A \left((-\mathbf{q}_{n_t}^T \bar{\mathbf{R}}_v^T \mathbf{u}_0 + \mathbf{D}_{k,n_t} \bar{\mathbf{R}}_v \mathbf{u}_0) \|\mathbf{D}_{k,n_t}\|^2 + \mathbf{D}_{k,n_t}^T \mathbf{u}^T \mathbf{D}_{k,n_t} \bar{\mathbf{R}}_v \mathbf{q}_{n_t} \right)}{2[h_k]_{n_t} \|\mathbf{D}_{k,n_t}\|^3} [\mathbf{a}(\boldsymbol{\varpi}^t)]_{n_t} + [h_k]_{n_t} \left(-j \frac{2\pi}{\lambda} \mathbf{P}_k^T \bar{\mathbf{R}}_v \mathbf{q}_{n_t} \right) [\mathbf{a}(\boldsymbol{\varpi}^t)]_{n_t}, \quad (57)$$

$$\frac{\partial \mathcal{F}_{1,k}(\tilde{\Lambda})}{\partial \tilde{\Lambda}} = 2\Re \left\{ \boldsymbol{\xi}_k^c \left(\frac{\partial \mathbf{h}_k}{\partial \tilde{\Lambda}} \right)^H \mathbf{F} \mathbf{w}_k \right\}, \quad (58)$$

$$\frac{\partial \mathcal{F}_{2,k,j}(\tilde{\Lambda})}{\partial \tilde{\Lambda}} = \left(\frac{\partial \mathbf{h}_k}{\partial \tilde{\Lambda}} \right)^H \tilde{\mathbf{A}}_j \mathbf{h}_k + \mathbf{h}_k^H \tilde{\mathbf{A}}_j \left(\frac{\partial \mathbf{h}_k}{\partial \tilde{\Lambda}} \right), \text{ where } \tilde{\mathbf{A}}_j = \mathbf{F} \mathbf{w}_j \mathbf{w}_j^H \mathbf{F}^H, \quad (59)$$

$$\frac{\partial \mathcal{F}_3(\tilde{\Lambda})}{\partial \tilde{\Lambda}} = 2\Re \left\{ \mathbf{u}^H \left(\frac{\partial \mathbf{G}_s}{\partial \tilde{\Lambda}} \right) \mathbf{F} \mathbf{W} \boldsymbol{\xi}^s \right\}, \quad (60)$$

$$\frac{\partial \mathcal{F}_{4,c}(\tilde{\Lambda})}{\partial \tilde{\Lambda}} = |\zeta_c|^2 \left(\mathbf{u}^H \left(\frac{\partial \mathbf{G}_c}{\partial \tilde{\Lambda}} \right) \tilde{\mathbf{A}} \mathbf{G}_c \mathbf{u} + \mathbf{u}^H \mathbf{G}_c \tilde{\mathbf{A}} \left(\frac{\partial \mathbf{G}_c}{\partial \tilde{\Lambda}} \right)^H \mathbf{u} \right), \text{ where } \frac{\partial \mathbf{G}_c}{\partial \tilde{\Lambda}} = \beta_c \mathbf{g}_c \left(\frac{\partial \mathbf{h}_c}{\partial \tilde{\Lambda}} \right)^H, \quad (61)$$

$$\frac{\partial \mathcal{F}_5(\tilde{\Lambda})}{\partial \tilde{\Lambda}} = |\zeta_s|^2 \left(\mathbf{u}^H \left(\frac{\partial \mathbf{G}_s}{\partial \tilde{\Lambda}} \right) \tilde{\mathbf{A}} \mathbf{G}_s \mathbf{u} + \mathbf{u}^H \mathbf{G}_s \tilde{\mathbf{A}} \left(\frac{\partial \mathbf{G}_s}{\partial \tilde{\Lambda}} \right)^H \mathbf{u} \right), \text{ where } \tilde{\mathbf{A}} = \mathbf{F} \mathbf{W} \mathbf{W}^H \mathbf{F}^H, \quad (62)$$

complexity for optimizing transmit digital beamformer \mathbf{W} and transmit analog beamformer \mathbf{F} is both $\mathcal{O}(N_t^3)$. To update the auxiliary variables μ , ξ^c and ξ_s , the complexities are $\mathcal{O}(KN_t)$, $\mathcal{O}(KN_t + K^2)$ and $\mathcal{O}(N_t K^2)$, respectively. The complexity for updating Λ mainly stems from the derivative calculations (51) for the L elements in Λ . Thus, the computational complexity of Λ is $\mathbf{O}(I_{GA}LN_t^2K^2)$, where I_{GA} is the number of iteration for gradient ascent. Considering the dominant computational steps, the total computational complexity of **Algorithm 2** is $\mathcal{O}(I_{AO}I_{GA}LN_t^2K^2)$, where I_{AO} denote the number of iterations of AO algorithm.

IV. NUMERICAL RESULTS

In this section, we will elaborate on the simulation setup and discussion of the numerical results to evaluate the performance of the proposed algorithm.

A. Simulation Setup

In the simulation, we set the BS as the origin of the global coordinate system. The center coordinates of the transmitting uniform planar array (UPA) and the receiving UPA are set to $[0, 0, -d_0]^T$ and $[0, 0, d_0]^T$, respectively. We assume the BS is equipped with N_t transmit antennas, N_r receive antennas, and N_{RF} RF chains. Each RF chain is connected to M antennas via analog phase shifters. The antenna's positions are set according to the transmit and receive UPAs with the largest achievable apertures $D \times D$. For each UPA, the plate size is $D \times D$ with $D = 10\lambda$. The BS operates at a carrier frequency of 30GHz. It serves $K = 4$ users, sensing $s = 1$ target, and there are $C = 3$ clutters in the scenario. The users and clutters are randomly distributed in front of the BS, i.e., $\phi_d \sim \mathcal{U}(-\frac{\pi}{2}, \frac{\pi}{2})$, and $\theta_d \sim \mathcal{U}(0, \pi)$ for $d \in \{1, \dots, K + C\}$. The sensing target is assumed to be located at $(\frac{\pi}{3}, \frac{\pi}{3})$. The reflection coefficients of both the target and the clutter, ζ_k and ζ_s , are set to 2 dB. In addition, the power budget at the BS is set as $P_{max} = 0$ dBm. The average noise power as $\sigma_k^2 = \sigma_s^2 = -80$ dBm. The penalty factor $\eta = 10$. The preliminary step size $\kappa = 100$ and the minimum step size $\kappa_{min} = 0.01$. It is worth noting that, unless otherwise specified, the rotation variable Λ we optimized includes all rotation parameters of the Tx and Rx, i.e., $\Lambda = [\alpha^t, \beta^t, \gamma^t, \alpha^r, \beta^r, \gamma^r]$. We perform 200 Monte Carlo simulations for the following results. The simulation parameters for the proposed system are listed in Table I.

To verify the effectiveness of the proposed scheme with Algorithm 2, we introduce five baselines to compare the performance improvement of our algorithm, which are: 1) Tx and Rx have fixed rotation angles, with RF chains adopting a sub-connected structure (**FPA, Sub-connected**), 2) Tx and Rx have fixed rotation angles, with RF chains adopting a fully-connected structure (**FPA, Fully-connected**), 3) Tx and Rx have fixed rotation angles, using a fully-digital beamformer (**FPA, Fully-digital**), 4) Tx and Rx can execute 3D rotations, with RF chains adopting a fully-connected structure (**RMA, Fully-connected**),

TABLE I: System Parameters

Parameters	Value
Number of antennas at the BS	$N_t = N_r = 16$
Number of users	$K = 4$
Number of clutters	$C = 3$
Wavelength	$\lambda = 0.01$ m
Size of antenna array	$D = 10\lambda$
Number of RF chains	$N_{RF} = 8$
Penalty factor	$\eta = 10$
Preliminary step size	$\kappa = 100$
Minimum step size	$\kappa_{min} = 1$
Power budget	$P_{max} = 0$ dBm
Position variable of the UPA center	$d_0 = 2$ m
Average noise power for users & target	$\sigma_k^2 = \sigma_s^2 = -80$ dBm
Reflection coefficient for target & clutters	$\zeta_s = \zeta_c = 3$
Azimuth of users and clutters	$\phi_d \in (-\frac{\pi}{2}, \frac{\pi}{2})$
Elevation of users and clutters	$\theta_d \in (0, \pi)$
Location of the target	$(\phi_s, \theta_s) = (\frac{\pi}{3}, \frac{\pi}{3})$
Path loss of the users & target	$\rho = -30$ dB

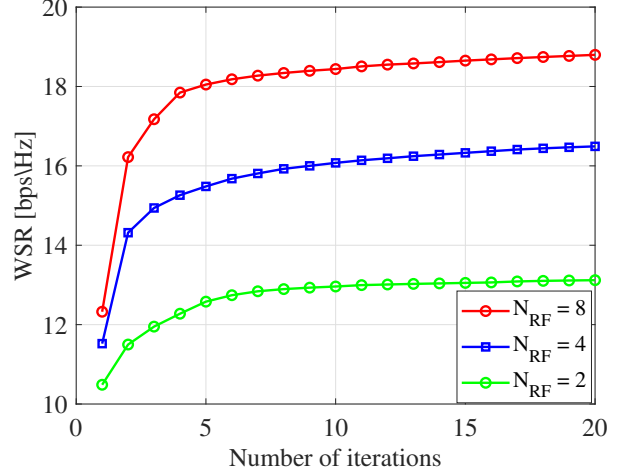


Fig. 2: Convergence evaluation of Algorithm 2. $N_t = N_r = 16$, $\varpi_c = 0.5$.

B. Convergence Evaluation

First, we evaluate the convergence of the proposed AO algorithm under different numbers of RF chains in Fig. 2. As can be seen, the algorithm converges rapidly in all scenarios, and the objective value tends to stabilize after 10 iterations. Moreover, the WSR increases as the number of RF chains increases. This is because the performance of the analog beamformer \mathbf{F} is constrained by the number of RF chains. Specifically, when the number of RF chains increases, the analog beamformer can achieve a higher DoFs to further enhance the overall system performance.

C. Beamfocusing of Algorithm 2

To verify the effect of Algorithm 2 on improving sensing performance, we consider the optimized beampattern by Algorithm 2 and compares it with the optimized beampattern by FPA scheme. This is to intuitively demonstrate the advantages

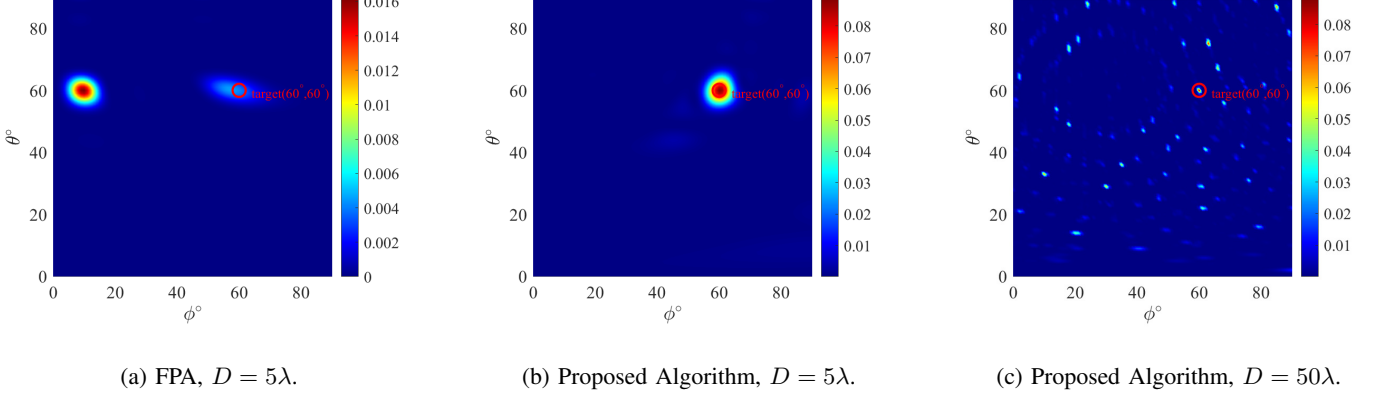


Fig. 3: Beampattern under different configurations

of rotatable array in the sensing function of ISAC system proposed in this paper. The beampattern at the angle (ϕ, θ) is computed as

$$\text{BP}(\phi, \theta) = \|\mathbf{u}^H \mathbf{G}_s(\phi, \theta) \mathbf{F} \mathbf{W}\|^2 \quad (65)$$

We set $\omega_s = 1$ to eliminate the interference from CUs. The number of transmit antennas and receive antennas are both $N_t = N_r = 16$, the number of RF chains is $N_{RF} = 4$, and the target is assumed to be located at $(60^\circ, 60^\circ)$. Figs.3(a) shows the optimized beampattern under the FPA scheme, from which it can be seen that the beam fails to focus well on the target position. In Figs.3(b), the side length of the UPA is set to $D = 5\lambda$, and it is observed that under the RA-aided scheme, the beam can focus precisely on the desired target position with extremely low interference to other positions. In the far-field scenario, as the side length of the UPA increases as shown in Fig.3(c), the width of the beam main lobe narrows gradually, however, due to the increase in the spacing between antennas in the array, the array periodicity is enhanced, the number of grating lobes increases, and thus more interference is generated.

D. Simulation Results

Fig. 4 compares the relationship between the WSR and the maximum transmit signal power P_{max} among different schemes. As shown in the figure, with the increase of transmit signal power, the WSR values of both the RA and FPA schemes keep rising, which is because a higher transmit power can enhance the signal strength. Under the condition that both the transmit power and precoding structure are the same, the performance of the RA scheme is consistently superior to that of the FPA scheme, which is attributed to the higher flexibility of the RA design in beamforming design. In addition, the analog precoding design with a fully-connected structure is always superior to that with a sub-connected structure, since all RF chains in the fully-connected structure are connected to all antenna elements through PS. It is noteworthy that when the power is less than -5 dBm, the WSR value of the RA scheme is better than that of the fully-digital beamforming design. This is due to the consideration of antenna aperture loss; at

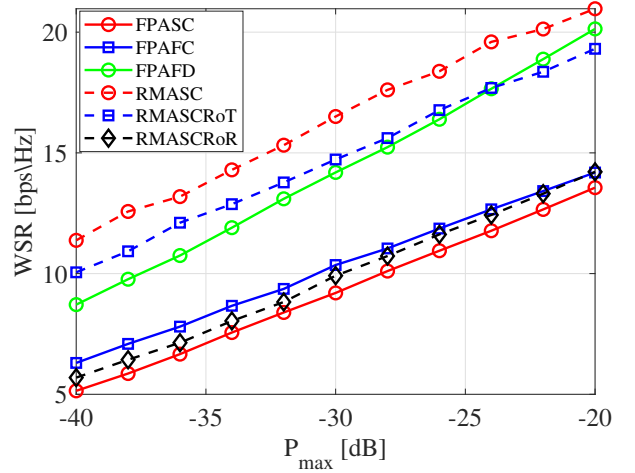


Fig. 4: WSR versus P_{max} . $N_t = N_r = 16$, $M = 4$, $\varpi_c = 0.5$.

low transmit power, the improvement of system performance mainly relies on antenna rotation. However, as the transmit signal power increases, the gain from beamforming becomes increasingly prominent and becomes the dominant factor driving the improvement of system performance, thus making the WSR lower than that of the fully-digital beamforming scheme.

Fig. 5 shows the relationship between the sensing rate and the maximum transmit power P_{max} under different schemes. We set $\omega_s = 1$, which means the ISAC system is sensing-focused. As can be seen from the figure, as P_{max} increases, the sensing rate of each schemes shows an upward trend. It can be intuitively observed from the figure that array rotation brings significant gain to sensing performance, and at the same time, the impact of different precoding structures on the sensing rate can also be clearly seen. Among them, the sensing rate of the fully digital beamforming scheme is lower than that of the RA scheme. This is because in the scenario where only a single target is sensed, the gain generated by array rotation is significantly greater than the beamforming gain.

Fig. 6 illustrates the the sum of communication rate versus

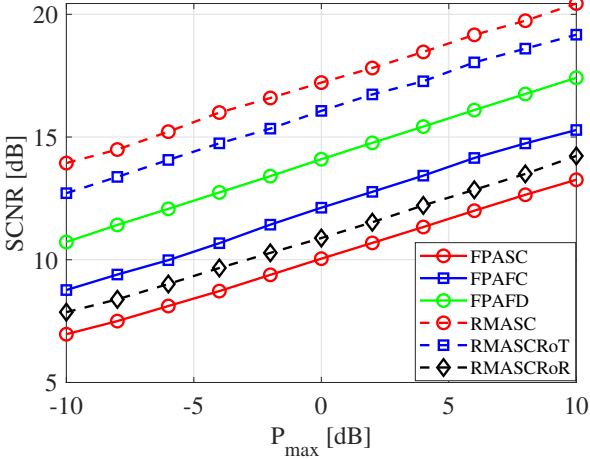


Fig. 5: Sensing rate versus P_{max} . $N_t = N_r = 16$, $M = 4$, $\varpi_s = 0.8$.

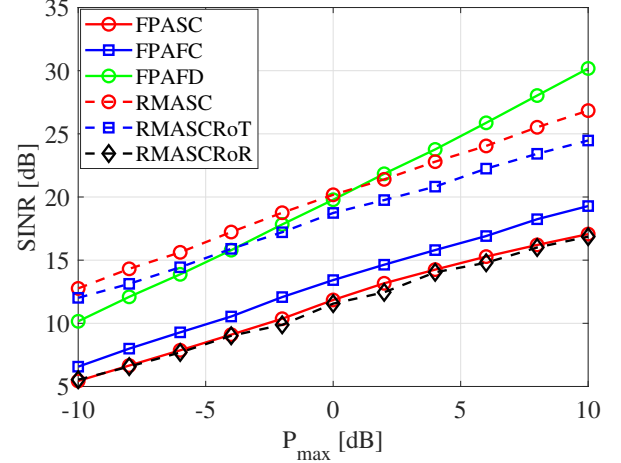


Fig. 6: Sum of communication rate versus P_{max} . $N_t = N_r = 16$, $M = 4$, $\varpi_c = 1$.

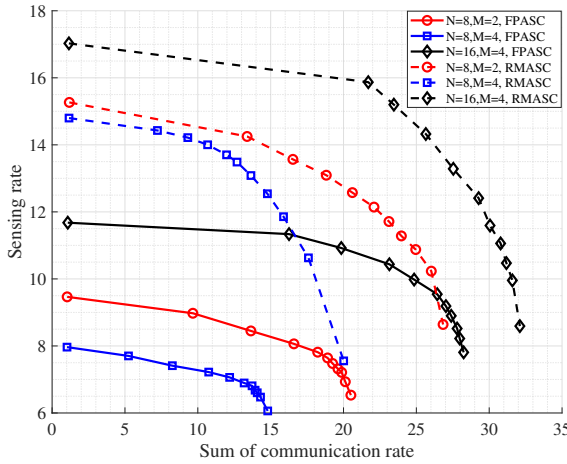


Fig. 7: Trade-off between sensing and communication performance.

the maximum transmit power P_{max} at a communication-focused ISAC with $\varpi_c = 1$. A similar trend with Fig. 5 can be observed, and the performance improvement on communication is more significant than that of sensing. Notably, when $P_{max} > 5$ dbm, the performance of the RA scheme with a sub-connected beamforming is lower than that of the FPA scheme with fully-connected beamforming. Because in the multi-user scenario, as the transmit power increases, the antenna rotation gain in the sub-connected structure is smaller than the beamforming gain in the fully-connected structure.

In Fig. 7, we analyze the trade-off between sensing and communication. We set $P_{max} = 0$ dbm, $D = 10\lambda$. By adjusting the sensing rate weight ϖ_s and the communication weight ϖ_c , the trade-off curves between the sensing rate and the communication rate are plotted. To analyze the impact of RA and sub-connected structure M on system performance, we consider three typical ISAC system configurations: 1) Number of transmit/receive antennas $N_t = N_r = 8, M = 2$; 2) $N_t = N_r = 8, M = 4$; 3) $N_t = N_r = 16, M = 2$. As shown in Fig. 7, under the condition of the same number of

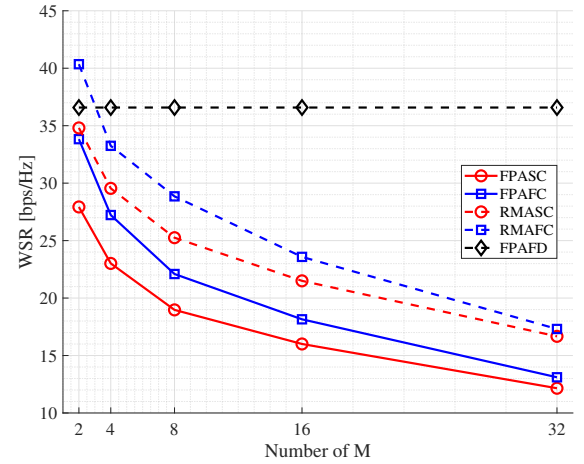


Fig. 8: WSR versus M . $N_t = N_r = 64$, $D = 10\lambda$, $\varpi_s = 0.7$.

antennas and M , the ISAC system adopting RA outperforms the FPA system in terms of the performance trade-off between communication and sensing. This is because RA can more accurately focus the beam on the desired position. Specifically, with a fixed number of antennas, more RF chains can enhance the DoF of beamforming but will increase hardware costs. While with a fixed M , more antennas need more RF chains to achieve an improvement in overall system performance. It is worth noting that when the sensing weight ϖ_s is large, the performance of RA-aided ISAC system schemes with fewer antennas is better than that of FPA schemes with more antennas. The reason is that RA can significantly improve the sensing performance of the system. As the ϖ_s decreases, the system is communication-focused. At this point, the performance of RA schemes with fewer antennas gradually becomes inferior to that of FPA scheme with more antennas. This is because the combination of an increased number of antennas and more RF chains provides higher DoF for beamforming, which is more suitable for the requirements of communication-focused ISAC. Hence, appropriate weighted factors and configuration

parameters need to be considered in partial engineering.

Finally, Figure. 8 illustrates the relationship between the WSR and the number of RF chains. We consider three system configurations: fully-connected hybrid beamforming, sub-connected hybrid beamforming, and fully digital beamforming. We set $N_t = N_r = 64$, $A = 10\lambda$, $\omega_c = 0.7$. It can be observed that as the M increases, the number of RF chains decreases correspondingly, and the WSR under the hybrid beamforming design show a downward trend. This can be explained from two perspectives. On one hand, an increased number of RF chains provides more DoFs for the downlink beamfocusing and thus mitigates the inter-user interference among CUs; On the other hand, with an increased number of RF chains, more sophisticated probing signal design can be achieved to realize better positioning performance. When the number of RF chains drops to a specific number, the performance of fully-connected and sub-connected hybrid precoding tends to be close, and at this time, RA becomes the main contributing factor to the system performance improvement.

V. CONCLUSION

In this paper, we study an RA-aided sub-connected hybrid beamforming design for ISAC systems. By jointly optimizing the angle of the rotatable array and the hybrid beamforming vector, we maximize the system's achievable WSR for both communications and sensing. We proposed an alternating optimization based framework for solving this non-convex optimization problem. We transform the objective function using the FP method, and alternately solve five sub-problems until the AO algorithm converges. We adopt the MMSE filtering method to optimize the receive beamformer. Then we derive the closed-form expressions for updating the digital and analog beamforming matrices. We propose a GA-based method to optimize the angle of the rotatable array. Simulation results verified the effectiveness of the proposed algorithm and the advantages of the considered RA-aided sub-connected structure ISAC scheme compared to FPA-based schemes. Remarkably, under some weight parameters, the performance of RA-aided ISAC system equipped with 8 transmit/receive antennas and 4 RF chains is outperformed to that of FPA ISAC system equipped with 16 transmit/receive antennas and 8 RF chains. This finding provides valuable insights for reducing hardware costs in engineering applications. In addition, apart from the sensing rate, this paper also derives and analyzes the sensing beampattern. The results show that RA can effectively optimize the beamfocusing effect and improve the sensing accuracy.

REFERENCES

- [1] F. Liu, C. Masouros, A. Li, H. Sun and L. Hanzo, "MU-MIMO Communications With MIMO Radar: From Co-Existence to Joint Transmission," *IEEE Trans. Wireless Commun.*, vol. 17, no. 4, pp. 2755-2770, Apr. 2018.
- [2] F. Liu *et al.*, "Integrated sensing and communications: Toward dual-functional wireless networks for 6G and beyond," *IEEE J. Sel. Areas Commun.*, vol. 40, no. 6, pp. 1728-1767, Jun. 2022.
- [3] F. Liu, C. Masouros, A. P. Petropulu, H. Griffiths and L. Hanzo, "Joint Radar and Communication Design: Applications, State-of-the-Art, and the Road Ahead," *IEEE Trans. Commun.*, vol. 68, no. 6, pp. 3834-3862, Jun. 2020.
- [4] Y. Sun, H. Xu, B. Ning, Z. Cheng, C. Ouyang and H. Yang, "Sum-Rate Optimization for RIS-Aided Multiuser Communications With Movable Antennas," *IEEE Wireless Commun. Lett.*, vol. 14, no. 2, pp. 450-454, Feb. 2025.
- [5] Y. He, Y. Cai, H. Mao and G. Yu, "RIS-Assisted Communication Radar Coexistence: Joint Beamforming Design and Analysis," *IEEE J. Sel. Areas Commun.*, vol. 40, no. 7, pp. 2131-2145, Jul. 2022.
- [6] K. Meng *et al.*, "UAV-Enabled Integrated Sensing and Communication: Opportunities and Challenges," *IEEE Wireless Commun.*, vol. 31, no. 2, pp. 97-104, Apr. 2024.
- [7] Z. Wang, Y. Liu, X. Mu, Z. Ding and O. A. Dobre, "NOMA Empowered Integrated Sensing and Communication," *IEEE Commun. Lett.*, vol. 26, no. 3, pp. 677-681, Mar. 2022.
- [8] W. Lyu *et al.*, "Hybrid NOMA Assisted Integrated Sensing and Communication via RIS," *IEEE Trans. Veh. Technol.*, vol. 73, no. 5, pp. 7368-7373, May 2024.
- [9] X. Yu, J. -C. Shen, J. Zhang and K. B. Letaief, "Alternating Minimization Algorithms for Hybrid Precoding in Millimeter Wave MIMO Systems," *IEEE J. Sel. Topics Signal Process.*, vol. 10, no. 3, pp. 485-500, Apr. 2016.
- [10] S. S. Ioushua and Y. C. Eldar, "A Family of Hybrid Analog-Digital Beamforming Methods for Massive MIMO Systems," *IEEE Trans. Signal Process.*, vol. 67, no. 12, pp. 3243-3257, 15 Jun., 2019.
- [11] J. Du, W. Xu, H. Shen, X. Dong and C. Zhao, "Hybrid Precoding Architecture for Massive Multiuser MIMO With Dissipation: Sub-Connected or Fully Connected Structures?," *IEEE Trans. Wireless Commun.*, vol. 17, no. 8, pp. 5465-5479, Aug. 2018.
- [12] X. Wang, Z. Fei, J. A. Zhang and J. Xu, "Partially-Connected Hybrid Beamforming Design for Integrated Sensing and Communication Systems," *IEEE Trans. Commun.*, vol. 70, no. 10, pp. 6648-6660, Oct. 2022.
- [13] W. Zhu, H. D. Tuan, E. Dutkiewicz, H. V. Poor and L. Hanzo, "Max-Min Rate Optimization of Low-Complexity Hybrid Multi-User Beamforming Maintaining Rate-Fairness," *IEEE Trans. Wireless Commun.*, vol. 23, no. 6, pp. 5648-5662, Jun. 2024.
- [14] J. An, H. Li, D. W. K. Ng and C. Yuen, "Fundamental Detection Probability vs. Achievable Rate Tradeoff in Integrated Sensing and Communication Systems," *IEEE Trans. Wireless Commun.*, vol. 22, no. 12, pp. 9835-9853, Dec. 2023.
- [15] L. Zhu, W. Ma and R. Zhang, "Movable Antennas for Wireless Communication: Opportunities and Challenges," *IEEE Commun. Mag.*, vol. 62, no. 6, pp. 114-120, Jun. 2024.
- [16] X. Shao, R. Zhang, Q. Jiang and R. Schober, "6D Movable Antenna Enhanced Wireless Network via Discrete Position and Rotation Optimization," *IEEE J. Sel. Areas Commun.*, vol. 43, no. 3, pp. 674-687, Mar. 2025.
- [17] X. Shao and R. Zhang, "6DMA Enhanced Wireless Network with Flexible Antenna Position and Rotation: Opportunities and Challenges," *IEEE Commun. Mag.*, vol. 63, no. 4, pp. 121-128, Apr. 2025.
- [18] X. Shao, R. Zhang, Q. Jiang, J. Park, T. Q. S. Quek and R. Schober, "Distributed Channel Estimation and Optimization for 6D Movable Antenna: Unveiling Directional Sparsity," *IEEE J. Sel. Topics Signal Processing*, vol. 19, no. 2, pp. 349-365, March 2025.
- [19] X. Shao, Q. Jiang and R. Zhang, "6D Movable Antenna Based on User Distribution: Modeling and Optimization," *IEEE Trans. Wireless Commun.*, vol. 24, no. 1, pp. 355-370, Jan. 2025.
- [20] L. Zhu, W. Ma and R. Zhang, "Modeling and Performance Analysis for Movable Antenna Enabled Wireless Communications," *IEEE Trans. Wireless Commun.*, vol. 23, no. 6, pp. 6234-6250, Jun. 2024.
- [21] J. Ding, Z. Zhou, X. Shao, B. Jiao and R. Zhang, "Movable Antenna-Aided Near-Field Integrated Sensing and Communication," *IEEE Trans. Wireless Commun.*, early access, 2025.
- [22] W. Lyu, S. Yang, Y. Xiu, Z. Zhang, C. Assi and C. Yuen, "Movable Antenna Enabled Integrated Sensing and Communication," *IEEE Trans. Wireless Commun.*, vol. 24, no. 4, pp. 2862-2875, Apr. 2025.
- [23] Y. Zhang *et al.*, "Movable Antenna-Aided Hybrid Beamforming for Multi-User Communications," *IEEE Trans. Veh. Technol.*, vol. 74, no. 6, pp. 9899-9903, Jun. 2025.
- [24] Y. Zhang, Y. Zhang, S. Xiao, W. Tang and Y. C. Eldar, "6D Movable Antenna-Aided Hybrid Beamforming for Multi-User Communications," *IEEE Globecom Workshops (GC Wkshps)*, Cape Town, South Africa, 2024, pp. 1-6.
- [25] Y. Sun, H. Xu, C. Ouyang and H. Yang, "Rotatable and Movable Antenna-Enabled Near-Field Integrated Sensing and Communication," *IEEE Internet Things J.*, early access, 2025.
- [26] D. Galappaththige, S. Zargari, C. Tellambura and G. Y. Li, "Near-Field ISAC: Beamforming for Multi-Target Detection," *IEEE Wireless Commun. Lett.*, vol. 13, no. 7, pp. 1938-1942, Jul. 2024.

- [27] Y. Sun, H. Xu, B. Ning, Z. Cheng, C. Ouyang and H. Yang, "Sum-Rate Optimization for RIS-Aided Multiuser Communications With Movable Antennas," *IEEE Wireless Commun. Lett.*, vol. 14, no. 2, pp. 450-454, Feb. 2025.
- [28] Z. Wang, X. Mu and Y. Liu, "Near-Field Integrated Sensing and Communications," *IEEE Commun. Lett.*, vol. 27, no. 8, pp. 2048-2052, Aug. 2023.
- [29] C. Ouyang, Y. Liu, H. Yang and N. Al-Dhahir, "Integrated Sensing and Communications: A Mutual Information-Based Framework," *IEEE Commun. Mag.*, vol. 61, no. 5, pp. 26-32, May 2023.
- [30] Y. Peng et al., "Mutual Information-Based Integrated Sensing and Communications: A WMMSE Framework," *IEEE Wireless Commun. Lett.*, vol. 13, no. 10, pp. 2642-2646, Oct. 2024.
- [31] X. Wang, Z. Fei, J. Huang and H. Yu, "Joint Waveform and Discrete Phase Shift Design for RIS-Assisted Integrated Sensing and Communication System Under Cramer-Rao Bound Constraint," *IEEE Trans. on Veh. Technol.*, vol. 71, no. 1, pp. 1004-1009, Jan. 2022.
- [32] K. Shen and W. Yu, "Fractional Programming for Communication Systems—Part I: Power Control and Beamforming," *IEEE Trans. Signal Process.*, vol. 66, no. 10, pp. 2616-2630, 15 May 15, 2018.
- [33] G. H. Golub and C. F. Van Loan, *Matrix Computations*, 3rd ed. Baltimore, MD, USA: The Johns Hopkins Univ. Press, 1996.
- [34] C. Pan et al., "Intelligent Reflecting Surface Aided MIMO Broadcasting for Simultaneous Wireless Information and Power Transfer," *IEEE J. Sel. Areas Commun.*, vol. 38, no. 8, pp. 1719-1734, Aug. 2020.